Enhanced Thermopower of Graphene Films with Oxygen Plasma Treatment

Ni Xiao,[†] Xiaochen Dong,[‡] Li Song,[§] Dayong Liu,[†,⊥] YeeYan Tay,[†] Shixin Wu,[†] Lain-Jong Li,[†] Yang Zhao,[†] Ting Yu,[¶] Hua Zhang,[†] Wei Huang,[‡] Huey Hoon Hng,[†] Pulickel M. Ajayan,[§,*] and Qingyu Yan[†,*]

[†]School of Materials Science and Engineering, Nanyang Technological University, 50 Nanyang Ave, Singapore 637819, Singapore, [‡]Key laboratory for Organic Electronic & Information Displays, Institute of Advanced Materials, Nanjing University of Posts and Telecommunications, 9 Wenyuan Road, Nanjing 210046, PR China, [§]Department of Mechanical Engineering & Materials Science, Rice University, 6100 Main Street, Houston, Texas 77005, United States , [⊥]Key Laboratory of Materials Physics, Institute of Solid State Physics, Chinese Academy of Sciences, P.O. Box 1129, Hefei 230031, People's Republic of China, and [¶]School of Physical and Mathematical Science, Nanyang Technological University, Singapore 637371, Singapore

ABSTRACT In this work, we show that the maximum thermopower of few layers graphene (FLG) films could be greatly enhanced up to ~700 μV/K after oxygen plasma treatment. The electrical conductivities of these plasma treated FLG films remain high, for example, ~10^4 S/m, which results in power factors as high as ~4.5×10^{-3} W K^{-2} m^{-1}. In comparison, the pristine FLG films show a maximum thermopower of ~80 μV/K with an electrical conductivity of ~5×10^4 S/m. The proposed mechanism is due to generation of local disordered carbon that opens the band gap. Measured thermopowers of single-layer graphene (SLG) films and reduced graphene oxide (rGO) films were in the range of −40 to 50 and −10 to 20 μV/K, respectively. However, such oxygen plasma treatment is not suitable for SLG and rGO films. The SLG films were easily destroyed during the treatment while the electrical conductivity of rGO films is too low.

KEYWORDS: graphene film · oxygen plasma · thermopower

Graphene,[1] the one atomic sp^2-bonded planar carbon sheet, has inspired considerable research in its fundamental intrinsic properties[2,3] and its potential applications in sensor,[4−9] transistor,[10−13] and solar cell.[14−16] Recently, the thermoelectric property of graphene became a rising research topic[17−24] because of its promising applications. Previous theoretical work on graphene demonstrated that the calculated thermoelectric figure of merit,[17−19] *ZT*, could be tuned to be as high as above 4.[20,21] Here, *ZT* is formulated as $ZT = (S^2\sigma/\kappa)T$, where *S*, σ, *k*, and *T* are the thermopower (or Seebeck coefficient), electrical conductivity, thermal conductivity and temperature in Kelvin, respectively. However, the experimental results of the thermoelectric property of graphene or carbon nanotubes (CNTs) are not promising,[22−24] for example, *ZT* is normally in the order of ~10^{-2}. The main factors causing such low *ZT* values are the high thermal conductivity (lattice thermal conductivity) of graphene/CNTs and the extremely low thermopower, typically in the range of 30−80 μV/K.[20,22,23,25,26] In the former case, although the pristine graphene/CNTs are well-known to possess high thermal conductivities,[27−30] there are reports on experimental and theoretical approaches[20,24,31−35] to possibly reduce the thermal conductivity of processed graphene/CNTs. For example, the phonon thermal transmission could be suppressed orders of magnitude by increasing the degree of disorder.[21] For the latter issue, however, not much improvement has been developed. The reported maximum thermopower of graphene/CNTs is only ~80 μV/K.[36] The investigation on approaches of increasing the thermopower values of graphene sheets toward the theoretical prediction[20] may facilitate the further understanding of the intrinsic properties of this exciting material.

Here, we report the study on the temperature-dependent thermopower of few layers graphene (FLG) films before and after oxygen plasma treatment. We found that the maximum thermopower of the pristine FLG was ~80 μV/K in the temperature range 475−575 K with electrical conductivity of ~5×10^4 S/m. After oxygen plasma treatment, the maximum thermopower for the same sample could be greatly enhanced up to ~700 μV/K in the temperature range 475−575 K while the electrical conductivity maintained in the same order of magnitude ~10^4 S/m, which resulted in power factor as high as ~4.5×10^{-3} W K^{-2} m^{-1}. This corresponded to an increase in the power factor of 15 times higher for oxygen plasma treated FLG films. We also investigated the thermoelectric properties of single layer graphene (SLG) films and reduced graphene oxide (rGO) films, and their corresponding thermopower values were in the range of −40 to 50 and −10 to 20 μV/K,

* Address correspondence to Ajayan@rice.edu, AlexYan@ntu.edu.sg.

Received for review November 20, 2010 and accepted March 18, 2011.

Published online March 18, 2011
10.1021/nn2001849

respectively. However, the oxygen plasma treatment was not suitable for SLG and rGO films. The oxygen plasma treatment was very difficult to control for SLG films, which were destroyed easily during the process. For rGO films, the electrical conductivity was too low and the oxygen plasma treatment would further decrease it, which was not ideal to achieve a high power factor. On the basis of our modeling study, we proposed that oxygen plasma induced structural disorder could cause the opening of the band gap[37−42] leading to the enhancement of the thermopower of FLG films.

RESULTS AND DISCUSSION

The morphology of the as-prepared graphene films was characterized by optical microscopy and scanning electron microscopy (SEM) after being transferred onto SiO_2 (300 nm)/Si substrates. Figure 1a−d shows the optical images and SEM images of SLG films and FLG films, respectively. The different color contrast between the graphene films and the SiO_2/Si substrate can be clearly observed, indicating the different thicknesses of the two films. In addition, these optical images display that these graphene films are pretty continuous and fairly uniform up to a long-range. Wrinkles are observed in these films, which could come from the thermal stresses created during the cooling process of the substrate after growth as there is a large difference of thermal expansion coefficients for Cu and graphene.[43] The AFM images and the height profiles of SLG and FLG films (see Figure S1 in the Supporting Information) reveal that the thickness of these two graphene films are around 1 nm for SLG films and 6 nm for FLG films, respectively. Figure 1e shows the typical Raman spectra obtained from the graphene films. The second-order Raman band located at 2650 cm^{-1} (2D peak) can be used to indicate the number of layers of graphene films by comparing its relative intensity with respect to that of the G peak located at 1680 cm^{-1}.[44] As shown by the bottom spectrum in Figure 1e, the intensity of the 2D peak is about twice of that of the G peak, signifying that the graphene films are only one or two layers. For the top spectrum in Figure 1e, the intensity of the 2D peak is much lower than that of the G peak, which suggests that the samples are multilayered. Meanwhile, the D peak at 1350 cm^{-1} is also observed in Figure 1e for the spectra of both SLG and FLG films. The intensity ratio between the D peak and the G peak, $I(D)/I(G)$, is higher for the FLG films than that of SLG films, which suggests more structural defects in the FLG films.

The thermoelectrical properties of these graphene films were investigated after they were transferred onto glass substrates by using the commercially available ZEM-3 system. The temperature-dependent thermopowers and the corresponding electrical conductivities for the SLG and FLG films are presented in Figure 2. Due to the delicate structure and high

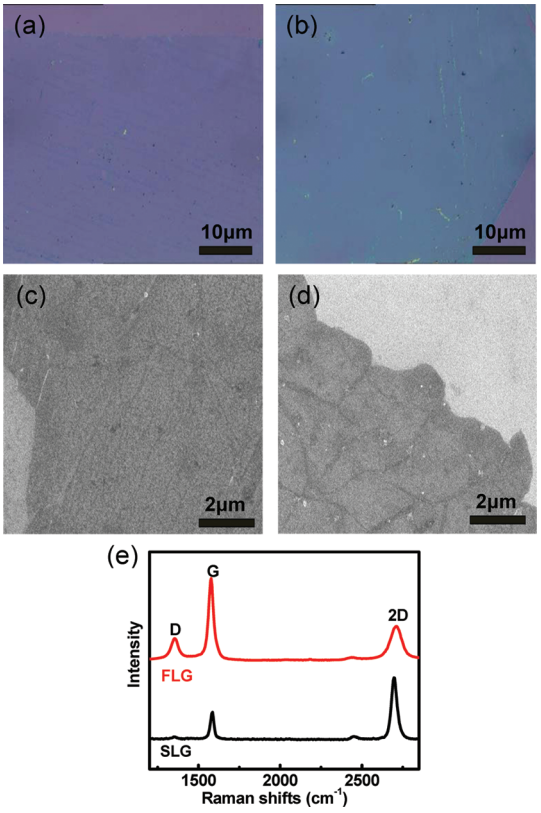

Figure 1. Characteristics of graphene films on SiO_2 (300 nm)/Si substrates. (a,b) Optical microscopy images of (a) SLG and (b) FLG films on SiO_2 (300 nm)/Si substrates. The different contrast between the substrate and graphene film shows the different thicknesses. (c,d) SEM images of (c) SLG and (d) FLG films on SiO_2 (300 nm) /Si substrates; (e) corresponding Raman spectra of the SLG and FLG films.

sensitivity of graphene films to environmental factors, the measurement temperatures were set up to 520 K for SLG films and 575 K for FLG films. The thermopowers of FLG films are p-type with "+" signs in the range of 40−80 μV/K at temperatures between 300 and 575 K. The maximum thermopower obtained on FLG films at 575 K is comparable to the highest reported values of thermopower of graphene samples.[36] The thermopowers of SLG films are in the narrow range of −40 to 50 μV/K and change from "+" to "−" (n-type) at 440 K. The p-type characteristics of SLG films at low temperature, for example, from 300 to 440 K, suggest that holes are the dominant carriers due to the easily adsorbed molecules (*e.g.*, oxygen or water) on the surface of SLG films.[45−47] At increased measurement temperature, desorption of such molecules leads to a decrease of holes concentration in the SLG films, which results in comparable concentration of both charge carriers. In this case, the sign of the thermopower is determined by the mobility of both the electrons and holes.[48] The transition of the thermopower of SLG films from "+" to "−" at 440 K indicates that the mobility of electrons is higher than that of the holes above this temperature, which makes electrons

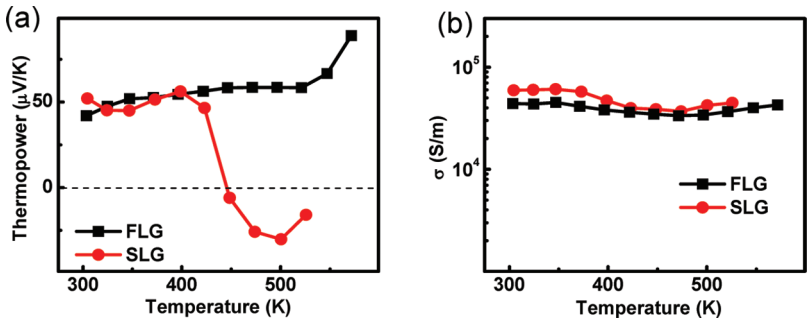

Figure 2. Thermolelectrical properties of graphene films. Temperature-dependent (a) thermopower and (b) electrical conductivity of SLG and FLG films on glass substrates.

become the dominant carriers. For the FLG films, there is no such sign change of the thermopower upon increasing the measurement temperature, which suggests holes are still the dominant charge carrier.

The electrical conductivity measurements by four-point probe using ZEM-3 show that the electrical conductivities of SLG films are in the range of $\sim 4 \times 10^4$ to $\sim 6 \times 10^4$ S/m, which is slightly higher than that of the FLG films, $\sim 4 \times 10^4$ to $\sim 5 \times 10^4$ S/m. As indicated from both the Raman spectra and thermoelectric results, the FLG films with a higher density of structural defects show a little higher thermopower as compared to that of the SLG films. It is therefore of interest to intentionally create more structural defects in the samples to investigate their thermoelectric properties. Here, we used oxygen plasma to treat the FLG films for different duration (10, 15, and 20 s) to create different extents of structural disorder in the samples.[49]

The morphology and atomic structure of the FLG films before and after plasma treatment were investigated with high resolution transmission electron microscopy (HRTEM) analysis. Figure 3a exhibits a HRTEM image of pristine FLG film, which shows an ordered lattice structure with a hexagonal symmetric point pattern as revealed by the selected area electron diffraction (SAED, inset in Figure 3a) analysis. The HRTEM image of plasma treated FLG film in Figure 3b reveals the relatively disordered lattice structure. The yellow circles highlight small crystals of carbon in such film while the red circles point out the disordered arrangement of carbon atoms. The SAED analysis (see inset in Figure 3b) showed diffused rings indicated no long-range ordering of the carbon atoms. Figure 3c depicts the Raman spectra of these FLG films with different oxygen plasma treatment durations. It is observed that I(D)/I(G) increases from 0.4 to 1.0 when the oxygen plasma treatment duration increases from 10 to 15 s, indicating the increased density of structural defects. For FLG films after plasma treatment for 20 s, it is found that the D, G, 2D peaks become broader and less distinguishable indicating that the ordered structure of the FLG films is damaged.

The thermopowers, electrical conductivities, and power factors of these oxygen plasma-treated FLG films are shown in Figure 3d–f. After 10 s treatment with oxygen plasma, the maximum thermopower of the FLG films within the measurement temperature range increases to 170 μV/K at 575 K as compared to 80 μV/K for pristine FLG films. Meanwhile, the electrical conductivity of the FLG films decreases by about ~30% to $\sim 2 \times 10^4$ to $\sim 3 \times 10^4$ S/m after such treatment process. Further increasing the treatment time to 15 s, we found that the maximum thermopower can be increased to ~700 μV/K at 575K while the electrical conductivity be decreased to 0.8×10^4 ~1×10^4 S/m. For FLG films after 20 s oxygen plasma treatment, the thermopower measurements could not be carried out as the electrical resistance was above the measurement range. It could be possibly due to (1) significant increase in the structural defects that increased the electrical resistivity of the FLG films or (2) the films became discontinuous after such treatment. Although the oxygen plasma treatment decreases the electrical conductivities of the FLG films, the power factors, denoted as $S^2\sigma$, increase significantly mainly because of the greatly enhanced thermopower (see Figure 3f), for example, 5.9×10^{-4} and 4.5×10^{-3} W K^{-2} m^{-1} for the 10-s and 15-s treated films as compared to 3.2×10^{-4} W K^{-2} m^{-1} for pristine FLG films. This corresponds to an increase in the power factor of 15 times higher for 15-s oxygen plasma treated FLG films than as for the pristine FLG films. We also performed oxygen plasma treatments on the SLG films. However, the process is much more difficult to control and most of the films became insulating after even a short duration of treatment.

Besides inducing structural disorder, the oxygen plasma treatment may also generate chemical functional groups, for example, –OH or –COOH, *etc.*, in the graphene films.[49] To examine the effects of these chemical functional groups on the thermoelectric properties of the graphene films, we further measured the thermopower and electrical conductivities of rGO films on glass substrates produced by Hummers method,[50] because it is well recognized that various chemical functional groups, for example, –OH or –COOH, *etc*, exist in the rGO films.[12,51–53]

The Raman spectrum of the rGO films (see Figure 4a) shows strong D peak with I(D)/I(G) = 1.45, which is

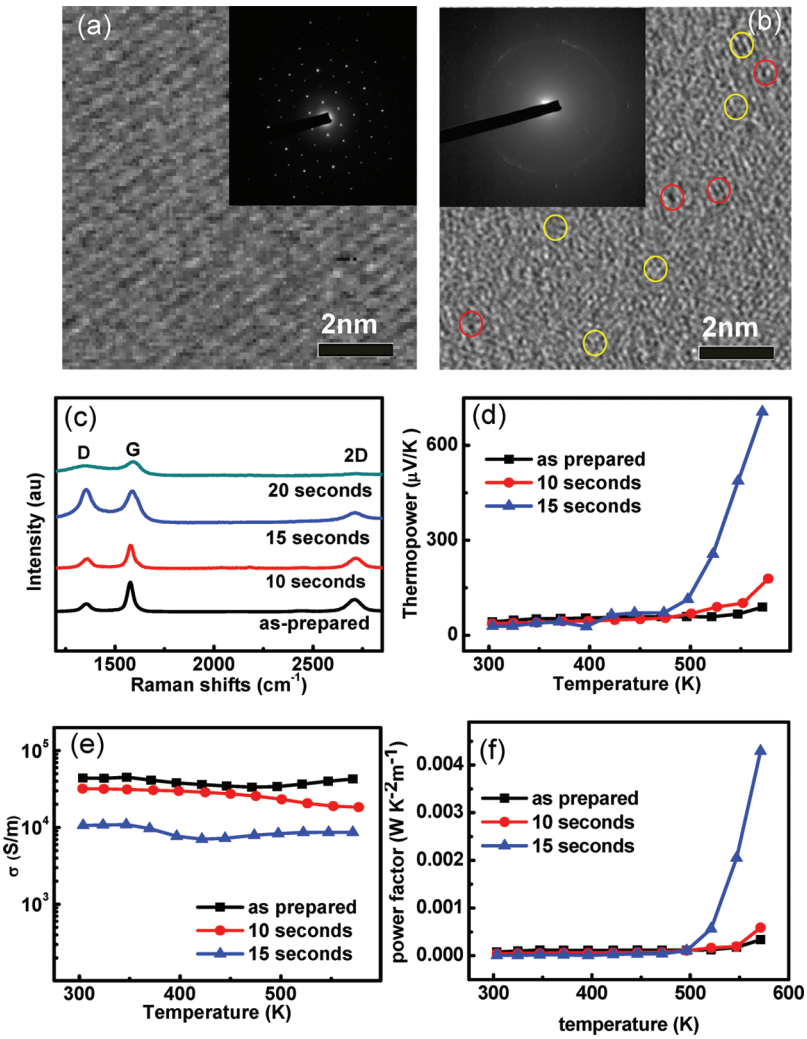

Figure 3. Atomic structure changes and thermoelectric properties before and after oxygen plasma treatment. (a,b) HRTEM images of FLG films (a) before and (b) after oxygen plasma treatment, illustrate that some atomic structures become disordered after oxygen plasma treatment. The yellow circles highlight small crystals of carbon in such films while the red circles point out the disordered arrangement of carbon atoms. The insets in panels a and b show the corresponding SAED pattern, which confirms the crystalline nature of the pristine FLG film and amorphous for samples after oxygen plasma treatment. (c) Raman spectra of the FLG film after 10, 15, and 20 s oxygen plasma treatment. (d–f) Temperature-dependent (d) thermopower, (e) electrical conductivity, and (f) power factor for the FLG films after different oxygen plasma treatments.

much higher than that of chemical vapor deposition (CVD) grown SLG and FLG films. As shown in Figure 4b, the thermopowers of rGO films are in the range of −10 to 20 μV/K with the electrical conductivity of 2×10^3 to 9×10^3 S/m. Since this electrical conductivity is already too low to achieve high power factors, we did not carry out oxygen plasma treatment on the rGO films, which may further decrease the electrical conductivity. The power factor calculated for rGO films is in the range of 0.8×10^{-6} to 3.6×10^{-6} W K^{-2} m^{-1}, which is about 3 orders of magnitude lower than that of FLG films after 15 s oxygen plasma treatment. The above observations indicate that those functional groups in rGO films may not be helpful in enhancing the thermopower. Thus, the significant enhancement in the thermopower of FLG films after oxygen plasma treatment is expected to be directly related to the generation of the structural defects/disorder.

We also considered the possibility of effect of substrates during the thermopower measurement. There is a report[54] that certain substrates become conducting at high temperature, which makes a dominant contribution to the measured thermopower and electrical conductivity of thin film samples such as conducting oxide and III–V films. We carried out measurements of the thermopower and electrical conductivity on the bare glass substrate in the temperature range of 525–600 K. The electrical resistance of the glass substrate was still above the measurement range, which indicated that the substrate remained insulating in this high temperature range and contributed little to measured thermoelectric properties of the graphene films.

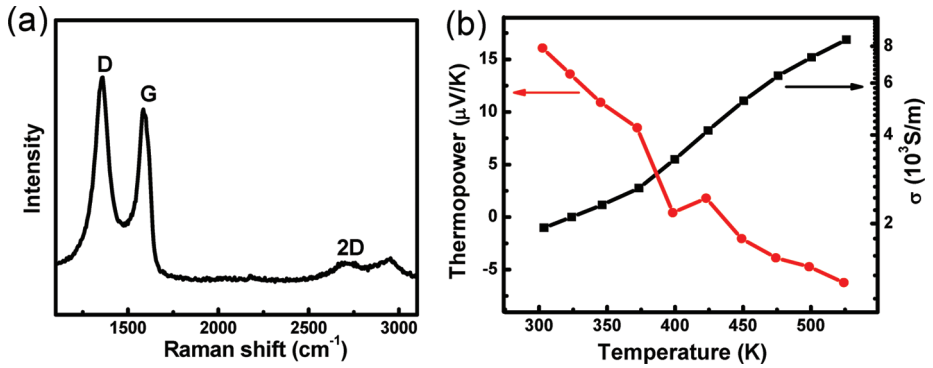

Figure 4. Characteristic and thermoelectrical properties of rGO: (a) Raman spectra of the rGO film; (b) temperature-dependent thermopower and electrical conductivity of the rGO film.

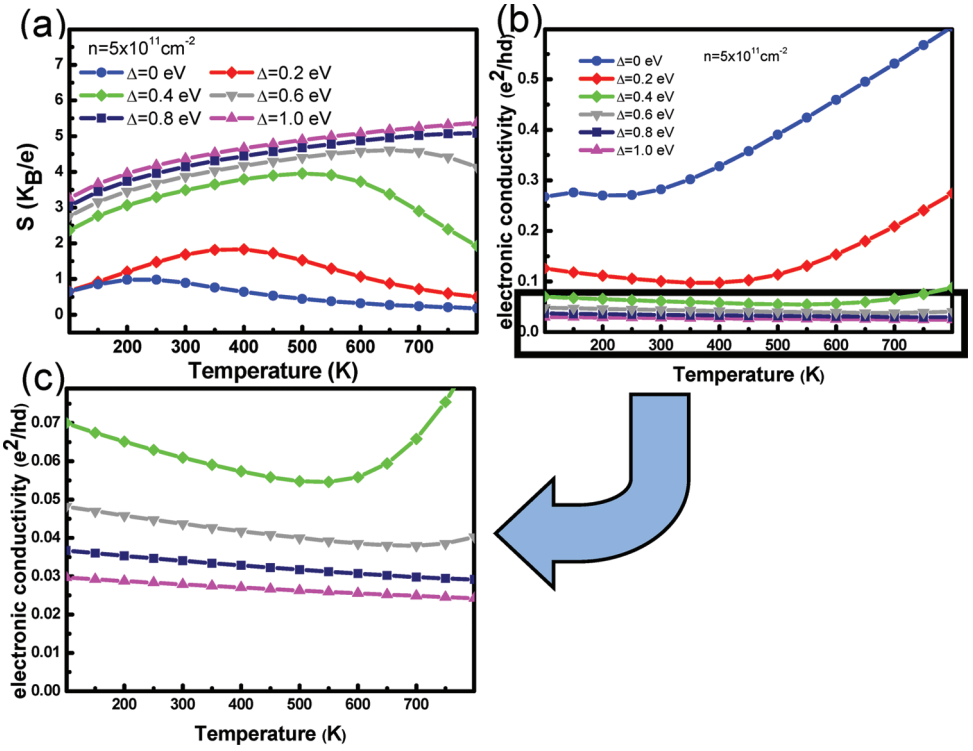

Figure 5. Plots of simulated (a) thermopower *vs* temperature and (b) electrical conductivity *vs* temperature for FLG films with different band gap values and a carrier concentration of $\sim 5 \times 10^{11}$ cm^{-2} based on the TB model. Graph c is the magnified plot of black box in graph b.

To understand the role of oxygen-plasma induced defects on the increase of the thermopower of graphene, we further simulate the model to explain the phenomena (see Supporting Information model simulation section). The modeling simulation results were plotted in Figure 5. Assuming a charge carrier density $n = 5 \times 10^{11}$ cm^{-2} without a gap open, the maximum value of thermopower is small, $\sim$ 86 μV/K (1 $K_B e \approx 86$ μV/K). Opening the band gap (see Supporting Information Figure S2) could lead to the great increase of the thermopower as displayed in Figure 5a. However, the simulated values could not match the experimental value exactly because of several factors that were not considered during the modeling part, such as a strong impurity scatter of the charge carriers. The simulated curves of electrical conductivities with such band gaps were also plotted (see Figure 5b). Note that the electrical conductivity is in the unit of e^2/hd ($\sim 1.14 \times 10^5$ S/m), where $d \approx$ 0.34 nm is the interlayer distance of the FLG films. The plot shows that the electrical conductivity decreases with increased band gaps. It also shows that the electrical conductivities with low band gaps, for example, from 0 to 1 ev, reduce less than 1 order of magnitude, which may give quality support of our experimental results.

CONCLUSIONS

We measured the thermopower of FLG films and found the thermopower of the FLG films could be

greatly enhanced by oxygen plasma treatment process in the temperature range of 475−575 K. After 15 s treatment, the maximum thermopower was ~700 μV/K at 575 K with electrical conductivity of ~1 × 10^4 S/m. This resulted in a power factor of 4.5 × 10^{-3} W K^{-2} m^{-1}, which is about 15 times higher than that of pristine FLG films. Further measurements on the rGO films showed very low thermopower. We attributed the greatly enhanced thermopower in the oxygen-plasma treated FLG films to the generation of structural disorders, which opened the $\pi-\pi^*$ gap.

EXPERIMENTAL SECTION

Preparation of FLG Films. FLG films were prepared on 25 μm thick Cu foils (purchased from Alfa Aesar) by the chemical vapor deposition (CVD) method with ethanol as precursor under atmosphere conditions. In a typical growth process, the Cu substrate was heated to 900 °C in the CVD chamber with Ar/H_2 (with flow rate of ~1000 sccm). Ethanol was introduced with H_2 flow (100 sccm) into the CVD chamber, and the flow was kept at 900 °C for 30 min. Finally, the Cu foil was cooled down under Ar/H_2 environment. After the growth of CVD graphene films, Cu foils with as-grown graphene films were spin-coated with a thin layer of PMMA (polymethylmetha-acrylate), and then the samples were immersed into iron nitrate solution to remove the Cu foil. The detached graphene films were transferred to the desired substrates, for example, silicon or glass. After transferring, the PMMA was removed using acetone. Finally the graphene on the desired substrate was washed using DI water and blow-dried gently with N_2 gas.

Preparation of SLG Films. SLG film was prepared on 25 μm thick Cu foils (purchased from Alfa Aesar) by chemical vapor deposition (CVD) method.[55] In a typical growth process, the Cu substrate was loaded in the CVD chamber and pumped to vacuum condition (10^{-2}Torr) before Ar/H_2 with a flow rate of ~400 sccm was introduced back into the chamber. Samples were heated to 950 °C at a pressure of ~8 to 9 Torr. The Ar/H_2 flow was then stopped and the hexane vapor at a rate of ~4 mL/h was introduced into the CVD chamber to keep the pressure of 500 mTorr for a few minutes. Finally, the Cu foil was cooled down under Ar/H_2 environment. The Cu foil etching and transfer procedures are the same as that for the FLG films as described above.

Preparation of rGO Film. Graphene oxide (GO) sheets were synthesized by a modified Hummer method using natural graphite as reported.[50] Then, the GO aqueous solution was spin-cast onto the glass substrates with thicknesses of ~15 nm. Finally, the GO sheets on glass substrates were reduced by hydrazine to rGO films.

Oxygen Plasma Treatment of FLG Films. The graphene films were treated with the plasma cleaner set consisting of PDC-32G and PDC-FMG plasmaflo (Harrick Plasma, USA). FLG films on glass substrates were directly exposed to plasma cleaner with oxygen/argon (1:10) mixture gas under low setting (input power, ~6.8 W) for a few seconds.

Characterization. The morphology and structure of graphene films were inspected by optical microscope, atomic force microscopy, and Raman spectroscopy. The optical images were obtained using a Nikon Eclipse Me 600 microscope. The AFM images were obtained using a Dimension 3100 (Veeco, CA, USA) in a tapping mode with a Si tip under ambient conditions. Raman spectra were obtained with a WITec CRM200 confocal Raman microscope (WITec Instruments Corp, Germany) using a 488 nm exciting radiation. TEM images of the samples were obtained by a using transmission electron microscopy (TEM) system (JEOL, model JEM-2100) operating at 200 kV.

Thermoelectric Properties Characterization. The thermopower and conductivity of graphene films on glass substrates were measured using a commercially available ZEM-3 Seebeck meter at a preselected temperature range from 300 to 550 K under a helium gas environment.

Acknowledgment. The authors gratefully acknowledge AcRF Tier 1 RG 31/08 of MOE (Singapore), NRF2009EWT-CERP001-026 (Singapore), Singapore A*STAR SERC Grant 1021700144 and Singapore Ministry of Education (MOE2010-T2-1-017) and (MOE Project No. T207B1214). H.Z. thanks the financial support from MOE of Singapore (ARC 10/10, No. MOE2010-T2-1-060). P.M.A. acknowledges support from the Office of Naval Research (ONR) through the MURI program, the Basic Energy Sciences division of the Department of Energy (DOE), and Rice University startup funds. L.S. is supported by DOE-BES program DE-SC0001479. Also financial support is received from the NSF of China (50902071, 61076067) and the 973 Program (China, 2009CB930601).

Supporting Information Available: Model simulation section, AFM images and height profiles of FLG and SLG films. This material is available free of charge *via* the Internet at http://pubs.acs.org.

REFERENCES AND NOTES

1. Novoselov, K. S.; Geim, A. K.; Morozov, S. V.; Jiang, D.; Zhang, Y.; Dubonos, S. V.; Grigorieva, I. V.; Firsov, A. A. Electric Field Effect in Atomically Thin Carbon Films. *Science* **2004,** *306*, 666–669.
2. Geim, A. K.; Novoselov, K. S. The Rise of Graphene. *Nat. Mater.* **2007,** *6*, 183–191.
3. Zhang, Y. B.; Tang, T. T.; Girit, C.; Hao, Z.; Martin, M. C.; Zettl, A.; Crommie, M. F.; Shen, Y. R.; Wang, F. Direct Observation of a Widely Tunable Bandgap in Bilayer Graphene. *Nature* **2009,** *459*, 820–823.
4. Dong, X. C.; Shi, Y. M.; Huang, W.; Chen, P.; Li, L. J. Electrical Detection of DNA Hybridization with Single-Base Specificity Using Transistors Based on CVD-Grown Graphene Sheets. *Adv. Mater.* **2010,** *22*, 1649–1653.
5. Schedin, F.; Geim, A. K.; Morozov, S. V.; Hill, E. W.; Blake, P.; Katsnelson, M. I.; Novoselov, K. S. Detection of Individual Gas Molecules Adsorbed on Graphene. *Nat. Mater.* **2007,** *6*, 652–655.
6. Mohanty, N.; Berry, V. Graphene-Based Single-Bacterium Resolution Biodevice and DNA Transistor: Interfacing Graphene Derivatives with Nanoscale and Microscale Biocomponents. *Nano Lett.* **2008,** *8*, 4469–4476.
7. Ang, P. K.; Chen, W.; Wee, A. T. S.; Loh, K. P. Solution-Gated Epitaxial Graphene as pH Sensor. *J. Am. Chem. Soc.* **2008,** *130*, 14392–14393.
8. Wang, Z. J.; Zhou, X. Z.; Zhang, J.; Boey, F.; Zhang, H. Direct Electrochemical Reduction of Single-Layer Graphene Oxide and Subsequent Functionalization with Glucose Oxidase. *J. Phys. Chem. C* **2009,** *113*, 14071–14075.
9. He, Q. Y.; Sudibya, H. G.; Yin, Z. Y.; Wu, S. X.; Li, H.; Boey, F.; Huang, W.; Chen, P.; Zhang, H. Centimeter-Long and Large-Scale Micropatterns of Reduced Graphene Oxide Films: Fabrication and Sensing Applications. *ACS Nano* **2010,** *4*, 3201–3208.
10. Li, X. L.; Wang, X. R.; Zhang, L.; Lee, S. W.; Dai, H. J. Chemically Derived, Ultrasmooth Graphene Nanoribbon Semiconductors. *Science* **2008,** *319*, 1229–1232.
11. Eda, G.; Fanchini, G.; Chhowalla, M. Large-Area Ultrathin Films of Reduced Graphene Oxide as a Transparent and Flexible Electronic Material. *Nat. Nanotechnol.* **2008,** *3*, 270–274.
12. Tung, V. C.; Allen, M. J.; Yang, Y.; Kaner, R. B. High-Throughput Solution Processing of Large-Scale Graphene. *Nat. Nanotechnol.* **2009,** *4*, 25–29.
13. Li, B.; Cao, X. H.; Ong, H. G.; Cheah, J. W.; Zhou, X. Z.; Yin, Z. Y.; Li, H.; Wang, J. L.; Boey, F.; Huang, W.; *et al*. All-Carbon

Electronic Devices Fabricated by Directly Grown Single-Walled Carbon Nanotubes on Reduced Graphene Oxide Electrodes. *Adv. Mater.* **2010,** *22*, 3058–3061.
14. Tang, Y. B.; Lee, C. S.; Xu, J.; Liu, Z. T.; Chen, Z. H.; He, Z. B.; Cao, Y. L.; Yuan, G. D.; Song, H. S.; Chen, L. M.; *et al*. Incorporation of Graphenes in Nanostructured TiO_2 Films *via* Molecular Grafting for Dye-Sensitized Solar Cell Application. *ACS Nano* **2010,** *4*, 3482–3488.
15. Valentini, L.; Cardinali, M.; Bon, S. B.; Bagnis, D.; Verdejo, R.; Lopez-Manchado, M. A.; Kenny, J. M. Use of Butylamine Modified Graphene Sheets in Polymer Solar Cells. *J. Mater. Chem.* **2010,** *20*, 995–1000.
16. Yin, Z. Y.; Wu, S. X.; Zhou, X. Z.; Huang, X.; Zhang, Q. C.; Boey, F.; Zhang, H. Electrochemical Deposition of ZnO Nanorods on Transparent Reduced Graphene Oxide Electrodes for Hybrid Solar Cells. *Small* **2010,** *6*, 307–312.
17. Sootsman, J. R.; Chung, D. Y.; Kanatzidis, M. G. New and Old Concepts in Thermoelectric Materials. *Angew. Chem., Int. Ed.* **2009,** *48*, 8616–8639.
18. Snyder, G. J.; Toberer, E. S. ComplexThermoelectric Materials. *Nat. Mater.* **2008,** *7*, 105–114.
19. Dresselhaus, M. S.; Chen, G.; Tang, M. Y.; Yang, R. G.; Lee, H.; Wang, D. Z.; Ren, Z. F.; Fleurial, J. P.; Gogna, P. New Directions for Low-Dimensional Thermoelectric Materials. *Adv. Mater.* **2007,** *19*, 1043–1053.
20. Ni, X. X.; Liang, G. C.; Wang, J. S.; Li, B. W. Disorder Enhances Thermoelectric Figure of Merit in Armchair Graphane Nanoribbons. *Appl. Phys. Lett.* **2009,** *95*, 192114.
21. Sevincli, H.; Cuniberti, G. Enhanced Thermoelectric Figure of Merit in Edge-Disordered Zigzag Graphene Nanoribbons. *Phys.Rev. B* **2010,** *81*, 113401.
22. Checkelsky, J. G.; Ong, N. P. Thermopower and Nernst Effect in Graphene in a Magnetic Field. *Phys. Rev. B* **2009,** *80*, 081413.
23. Wei, P.; Bao, W. Z.; Pu, Y.; Lau, C. N.; Shi, J. Anomalous Thermoelectric Transport of Dirac Particles in Graphene. *Phys. Rev. Lett.* **2009,** *102*, 166808.
24. Yao, Q.; Chen, L. D.; Zhang, W. Q.; Liufu, S. C.; Chen, X. H. Enhanced Thermoelectric Performance of Single-Walled Carbon Nanotubes/Polyaniline Hybrid Nanocomposites. *ACS Nano* **2010,** *4*, 2445–2451.
25. Ouyang, Y. J.; Guo, J. A Theoretical Study on Thermoelectric Properties of Graphene Nanoribbons. *Appl. Phys. Lett.* **2009,** *94*, 263107.
26. Zuev, Y. M.; Chang, W.; Kim, P. Thermoelectric and Magnetothermoelectric Transport Measurements of Graphene. *Phys. Rev. Lett.* **2009,** *102*, 096807.
27. Balandin, A. A.; Ghosh, S.; Bao, W. Z.; Calizo, I.; Teweldebrhan, D.; Miao, F.; Lau, C. N. Superior Thermal Conductivity of Single-Layer Graphene. *Nano Lett.* **2008,** *8*, 902–907.
28. Hu, J. N.; Ruan, X. L.; Chen, Y. P. Thermal Conductivity and Thermal Rectification in Graphene Nanoribbons: A Molecular Dynamics Study. *Nano Lett.* **2009,** *9*, 2730–2735.
29. Faugeras, C.; Faugeras, B.; Orlita, M.; Potemski, M.; Nair, R. R.; Geim, A. K. Thermal Conductivity of Graphene in Corbino Membrane Geometry. *ACS Nano* **2010,** *4*, 1889–1892.
30. Cai, W. W.; Moore, A. L.; Zhu, Y. W.; Li, X. S.; Chen, S. S.; Shi, L.; Ruoff, R. S. Thermal Transport in Suspended and Supported Monolayer Graphene Grown by Chemical Vapor Deposition. *Nano Lett.* **2010,** *10*, 1645–1651.
31. Chang, C. W.; Fennimore, A. M.; Afanasiev, A.; Okawa, D.; Ikuno, T.; Garcia, H.; Li, D. Y.; Majumdar, A.; Zettl, A. Isotope Effect on the Thermal Conductivity of Boron Nitride Nanotubes. *Phys. Rev. Lett.* **2006,** *97*, 085901.
32. Savic, I.; Mingo, N.; Stewart, D. A. Phonon Transport in Isotope-Disordered Carbon and Boron-Nitride Nanotubes: Is Localization Observable?. *Phys. Rev. Lett.* **2008,** *101*, 165502.
33. Stewart, D. A.; Savic, I.; Mingo, N. First-Principles Calculation of the Isotope Effect on Boron Nitride Nanotube Thermal Conductivity. *Nano Lett.* **2009,** *9*, 81–84.
34. Meng, C. Z.; Liu, C. H.; Fan, S. S. A Promising Approach to Enhanced Thermoelectric Properties Using Carbon Nanotube Networks. *Adv. Mater.* **2010,** *22*, 535–539.
35. Nika, D. L.; Pokatilov, E. P.; Askerov, A. S.; Balandin, A. A. Phonon Thermal Conduction in Graphene: Role of Umklapp and Edge Roughness Scattering. *Phys. Rev. B* **2009,** *79*, 155413.
36. Seol, J. H.; Jo, I.; Moore, A. L.; Lindsay, L.; Aitken, Z. H.; Pettes, M. T.; Li, X. S.; Yao, Z.; Huang, R.; Broido, D.; *et al*. Two-Dimensional Phonon Transport in Supported Graphene. *Science* **2010,** *328*, 213–216.
37. Denis, P. A. Band Gap Opening of Monolayer and Bilayer Graphene Doped with Aluminium, Silicon, Phosphorus, and Sulfur. *Chem. Phys. Lett.* **2010,** *492*, 251–257.
38. Coletti, C.; Riedl, C.; Lee, D. S.; Krauss, B.; Patthey, L.; von Klitzing, K.; Smet, J. H.; Starke, U. Charge Neutrality and Band-Gap Tuning of Epitaxial Graphene on SiC by Molecular Doping. *Phys. Rev. B* **2010,** *81*, 235401.
39. Bai, J. W.; Zhong, X.; Jiang, S.; Huang, Y.; Duan, X. F. Graphene Nanomesh. *Nat. Nanotechnol.* **2010,** *5*, 190–194.
40. Yang, C. K. Graphane with Defect or Transition-Metal Impurity. *Carbon* **2010,** *48*, 3901–3905.
41. Martinazzo, R.; Casolo, S.; Tantardini, G. F. Symmetry-Induced Band-Gap Opening in Graphene Superlattices. *Phys. Rev. B* **2010,** *81*, 245420.
42. Pujari, B. S.; Kanhere, D. G. Density Functional Investigations of Defect-Induced Mid-Gap States in Graphane. *J. Phys. Chem. C* **2009,** *113*, 21063–21067.
43. Chae, S. J.; Gunes, F.; Kim, K. K.; Kim, E. S.; Han, G. H.; Kim, S. M.; Shin, H. J.; Yoon, S. M.; Choi, J. Y.; Park, M. H.; *et al*. Synthesis of Large-Area Graphene Layers on Polynickel Substrate by Chemical Vapor Deposition: Wrinkle Formation. *Adv. Mater.* **2009,** *21*, 2328–2333.
44. Ni, Z. H.; Wang, H. M.; Kasim, J.; Fan, H. M.; Yu, T.; Wu, Y. H.; Feng, Y. P.; Shen, Z. X. Graphene Thickness Determination Using Reflection and Contrast Spectroscopy. *Nano Lett.* **2007,** *7*, 2758–2763.
45. Lee, G.; Lee, B.; Kim, J.; Cho, K. Ozone Adsorption on Graphene: *Ab Initio* Study and Experimental Validation. *J. Phys. Chem. C* **2009,** *113*, 14225–14229.
46. Leenaerts, O.; Partoens, B.; Peeters, F. M. Adsorption of Small Molecules on Graphene. *Microelectron. J.* **2009,** *40*, 860–862.
47. Huang, B.; Li, Z. Y.; Liu, Z. R.; Zhou, G.; Hao, S. G.; Wu, J.; Gu, B. L.; Duan, W. H. Adsorption of Gas Molecules on Graphene Nanoribbons and Its Implication for Nanoscale Molecule Sensor. *J. Phys. Chem. C* **2008,** *112*, 13442–13446.
48. Johnson, V. A.; Larkhorovitz, K. Theory of Thermoelectric Power in Semiconductor with Applications to Germunium. *Phys. Rev.* **1953,** *92*, 226–232.
49. Kim, D. C.; Jeon, D. Y.; Chung, H. J.; Woo, Y.; Shin, J. K.; Seo, S. The Structural and Electrical Evolution of Graphene by Oxygen Plasma-Induced Disorder. *Nanotechnology* **2009,** *20*, 375703.
50. Zhou, X. Z.; Huang, X.; Qi, X. Y.; Wu, S. X.; Xue, C.; Boey, F. Y. C.; Yan, Q. Y.; Chen, P.; Zhang, H. *In Situ* Synthesis of Metal Nanoparticles on Single-Layer Graphene Oxide and Reduced Graphene Oxide Surfaces. *J. Phys. Chem. C* **2009,** *113*, 10842–10846.
51. Park, S.; Ruoff, R. S. Chemical Methods for the Production of Graphenes. *Nat. Nanotechnol.* **2009,** *4*, 217–224.
52. Allen, M. J.; Fowler, J. D.; Tung, V. C.; Yang, Y.; Weiller, B. H.; Kaner, R. B. Temperature-Dependent Raman Spectroscopy of Chemically Derived Graphene. *Appl. Phys. Lett.* **2008,** *93*, 193119.
53. Fowler, J. D.; Allen, M. J.; Tung, V. C.; Yang, Y.; Kaner, R. B.; Weiller, B. H. Practical Chemical Sensors from Chemically Derived Graphene. *ACS Nano* **2009,** *3*, 301–306.
54. Bahk, J. H.; Zeng, G. H.; Zide, J. M. O.; Lu, H.; Singh, R.; Liang, D.; Ramu, A. T.; Burke, P.; Bian, Z. X.; Gossard, A. C.; Shakouri, A.; Bowers, J. E. High-Temperature Thermoelectric Characterization of III−V Semiconductor Thin Films by Oxide Bonding. *J. Electron. Mater.* **2010,** *39*, 1125–1132.
55. Srivastava, A.; Galande, C.; Ci, L.; Song, L.; Rai, C.; Jariwala, D.; Kelly, K. F.; Ajayan, P. M. Novel Liquid Precursor-Based Facile Synthesis of Large-Area Continuous, Single, and Few-Layer Graphene Films. *Chem. Mater.* **2010,** *22*, 3457–3461.